

Supporting Information

Activation of Natural Halloysite Nanotubes by Introducing Lanthanum Oxycarbonate Nanoparticles via Co-calcination for Outstanding Phosphate Removal

Yanfu Wei⁺, Peng Yuan^{+,*}, Dong Liu, Dusan Losic, Daoyong Tan, Fanrong Chen, Hongchang Liu, Junming Zhou, Peixin Du, Yaran Song

⁺These authors contributed equally to this work

E-mail: yuanpeng@gig.ac.cn

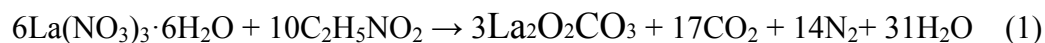
Table of Contents

<i>Experimental Procedures</i>	S2
Synthesis of LO-HNT.....	S2
Phosphate adsorption test	S2
Effluent sampling and analysis.....	S4
Characterization methods	S4
<i>Supplementary Results</i>	S7
Figure S1 XPS spectra of P@LO-HNT, LO-HNT and HNT	S7
Figure S2 FTIR spectra of LO, HNT, LO-HNT, P@LO-HNT and P@LO	S9
Figure S3 Cross-sectional TEM image and SAED pattern of LO-HNT	S11
Figure S4 Phosphate adsorption isotherms for HNT and calcined HNT.....	S12
Figure S5 Zeta potential of LO-HNT, Al ₂ O ₃ , HNT, and LO	S13
Figure S6 TEM images of LO nanoparticles.....	S14
Figure S7 Effect of heating temperature and mass ratio on phosphate removal	S15
Analysis for phosphate proportions of different states in LO-HNT	S16
Table S1 XRF result of LO-HNT and P@LO-HNT.....	S17
Table S2 The maximum phosphate adsorption capacity of La-supported materials ..	S18
Table S3 Langmuir parameters fitted for phosphate adsorption	S20
Table S4 Parameter of the domestic sewage effluent.....	S21
Table S5 Dose of reported phosphate adsorbents used in practical phosphate polluted samples	S22
<i>Supporting References</i>	S23

Experimental Procedures

Synthesis of LO-HNT

A certain amount of halloysite nanotube (HNT), lanthanum nitrate hexahydrate, and glycine were mixed in a 10 mL test tube. The solution was sonicated for 30 min after adding deionized water. The resulting suspension was evacuated for 30 min in a 250 mL filter flask. The procedure was followed by placing the suspension in an oven and drying at 120°C for 2 hours to obtain a dried sample. The product was then heated in a tube furnace under a nitrogen flow rate of 180 mL/min for 2 hours. The LO nanopartilces is formed through the glycine-nitrate combustion reaction between $\text{La}(\text{NO}_3)_3 \cdot 6\text{H}_2\text{O}$ and $\text{C}_2\text{H}_5\text{NO}_2$. The reaction is as follows:



After cooling, the sample went through a 200-mesh sieve to obtain the final lanthanum oxycarbonate ($\text{La}_2\text{O}_2\text{CO}_3$, abbreviated as LO) nanoparticle-coated HNT adsorbent (LO-HNT). The mass ratio of HNT/La and the heating temperature were optimized, as shown in Figure S7, and the LO-HNT sample prepared using 450°C calcination with a HNT/La mass ratio of 1/0.45 were used for adsorption experiments. HNT and HNT calcined at 450°C and 700°C as well as LO without supported material (synthesized at the same condition of LO-HNT) were used as control samples.

Phosphate adsorption test

To investigate the effect of mass ratio and calcination temperature of HNT/La on the adsorption of phosphate, the mass ratios of HNT/La were studied at 1/0.15, 1/0.3, and 1/0.45.

The effect of temperature was studied at 250, 350, 450, 550, and 650°C. The 50 mg of LO-HNT and 20 mL of KH_2PO_4 (230 and 700 mg P/L, calculated as P concentration) were mixed in a 50-mL centrifuge tube and placed on a shaker (250 rpm and 25°C) for 1 d. For kinetic studies, 50 mg of LO-HNT and 20 mL of KH_2PO_4 were mixed in a 50 mL centrifuge tube and placed in shaker (250 rpm and 25°C) under predetermined time intervals (0.33, 0.67, 1, 2, 4, 8, 16, 32, and 64 h) with a phosphate concentration of 700 mg P/L. Different concentrations of phosphate were used to evaluate the adsorption isotherms for phosphate on LO-HNT, pristine HNT, HNT calcined at 450°C and 700°C, and LO. The samples were shaken on a rotary shaker at 250 rpm and 25°C for 1 d. The pH of the solutions was maintained at 4.5 throughout the kinetic and isotherm adsorption.

To study the pH influence on phosphate capture, LO-HNT were mixed with 50 mg P/L phosphate solution at the adsorbent dose of 0.5 g/L. The initial pH value, ranging from 3.0 to 10.0, was adjusted by NaOH and/or HCl solutions. The effect of coexisting interfering compounds, e.g., organic matters and inorganic species on phosphate adsorption capacities were evaluated by dissolving 1 and 10 mM of Cl^- , NO_3^- , HCO_3^- , SO_4^{2-} or 1 and 10 mg/L of fulvic acid and humic acid into 50.0 mL of phosphate solution. The dosage of the LO-HNT was set among 0.01-1.0 g/L to determine the optimal value for completely phosphate removal. Besides, the contents of La^{3+} and Al^{3+} leakage was measured by using ICP-MS.

All samples were collected and centrifuged for 5 min at 8000 rpm for solid precipitate from the solution. The concentration of the phosphate in the solution was determined by phosphomolybdate blue. All tests were performed in triplicate. The adsorption performance, i.e., the quantity of phosphate adsorbed by per unit mass of the sample, Q_e (mg P/g), is calculated as follows:

$$Q_e = (C_i - C_e) V / M \quad (2)$$

in which Q_e is the adsorbed amount of phosphate (mg P/g); C_i is the initial concentration of phosphate (mg P/L); C_e is the equilibrium concentration of phosphate (mg P/L); M is the mass of the adsorbent (g); and V is the volume of the solution (L). The maximum adsorption capacity is the most important criteria, and it has high values that indicate efficient phosphate removal. We used the Langmuir model to fit the adsorption isotherm for phosphate removal.

$$C_e / q_e = 1 / Q_m \cdot K_L + C_e / Q_m \quad (3)$$

Here, C_e (mg P/L) is the equilibrium concentration of phosphate, and q_e (mg P/g) is the corresponding adsorbed amount of phosphate; Q_m (mg P/g) is the fitting parameter representing the maximum adsorption capacity, and K_L (L/mg) is the Langmuir constant.

Effluent sampling and analysis

The sewage effluent was sampled from a subsurface flow constructed wetlands within the campus of Guangzhou Institute of Geochemistry, Guangzhou City, China. The collected sample were saved in a refrigerator at 4°C. The samples were then filtered through a 0.22 μm filter membrane to separate the aqueous phase from suspended matters. Potassium dichromate method was used for chemical oxygen demand analysis, colorimetric method for ammonium (NH₄-N) and Nitrate nitrogen (NO₃-N) analysis. Total organic carbon (TOC) and total nitrogen were measured using a TOC/TN analyzer (TOC-VCPH, Shimadzu). Dissolved oxygen (DO) and pH were measured in situ using a portable multiparameter meter (Orion 5-star, Thermo).

Characterization methods

The X-ray powder diffraction patterns (XRD) were obtained on a Bruker D8 Advance diffractometer equipped with graphite monochromatized Cu K α radiation ($\lambda = 0.154\text{nm}$); the samples were HNT heated at 450°C, LO-HNT, and LO. The tube voltage is 40 kV with a tube current of 40 mA and a 1° 2 θ /min scan rate from 3 to 50°. The elemental contents in the LO-HNT and phosphate adsorbed LO-HNT (P@LO-HNT) were determined by XRF (Niton XL3t-800 X-ray fluorescence apparatus). Transmission electron microscopy (TEM) photomicrographs for LO-HNT samples were taken on a Titan Themis 200 TEM/STEM microscope at 200 kV. For characterizing the cross-sectional surface of the LO-HNT particle, ultra-thin sections of NKAol were made. LO-HNT was embedded in epoxy resin which was allowed to harden, followed by cutting with an ultra-microtome. The ultra-thin sections of LO-HNT were further analyzed using TEM and selected area electron diffraction at 200 kV. The scanning electron microscopy (SEM) images of HNT and LO-HNT were taken on a Hitachi 5200 SEM. The BET tests for HNT and LO-HNT were determined via a Micromeritics ASAP-2000 nitrogen adsorption apparatus. The Fourier transform infrared (FTIR) spectra of samples were collected with a Bruker Vertex-70 FTIR spectrometer from 4000 to 400 cm⁻¹ at room temperature. The zeta potential of LO-HNT, HNT, LO, and Al₂O₃ were performed using a Zetasizer Nano ZS90 (Malvern).

X-ray photoelectron spectroscopy (XPS) used a K-alpha electron spectrometer from VG Scientific using 300W Al K α radiation. The final concentrations of phosphate were detected on a UV spectrophotometer at 580 nm. The P@LO-HNT sample was prepared via an FIB-SEM (FEI 200). The morphology and elemental content distribution of P@LO-HNT were examined by STEM combined with energy-dispersive X-ray imaging (Titan Themis 200

TEM/EDX microscope). Phosphorus K-edge XANES spectra were collected on Beamline 4B7A at the Beijing Synchrotron Radiation Facility, China. The spectra were collected in fluorescence yield mode between -10 to $+40$ eV relative to the P K-edge energy at 2151 eV using a step size of 0.2 eV between 2140 eV and 2190 eV. XANES spectra for each sample were baseline corrected and normalized using the ATHENA program under IFEFFIT interface.^{1,2} The distribution of phosphate bonding between La and Al in P@LO-HNT samples was determined by linear combination fitting (LCF) analyses over the relative energy range of -10 to $+40$ eV using the Athena program. The P@LO-HNT sample used for XRF, XPS, FTIR, FIB-SEM, and XANES analysis were prepared by mixing LO-HNT with phosphate at 1000 mg P/L for 1 d at pH of 4.5. Samples of phosphate adsorbed on LO and Al₂O₃ at 1000 mg P/L and 600 mg P/L were used as standards in LCF analysis.

Supplementary Results

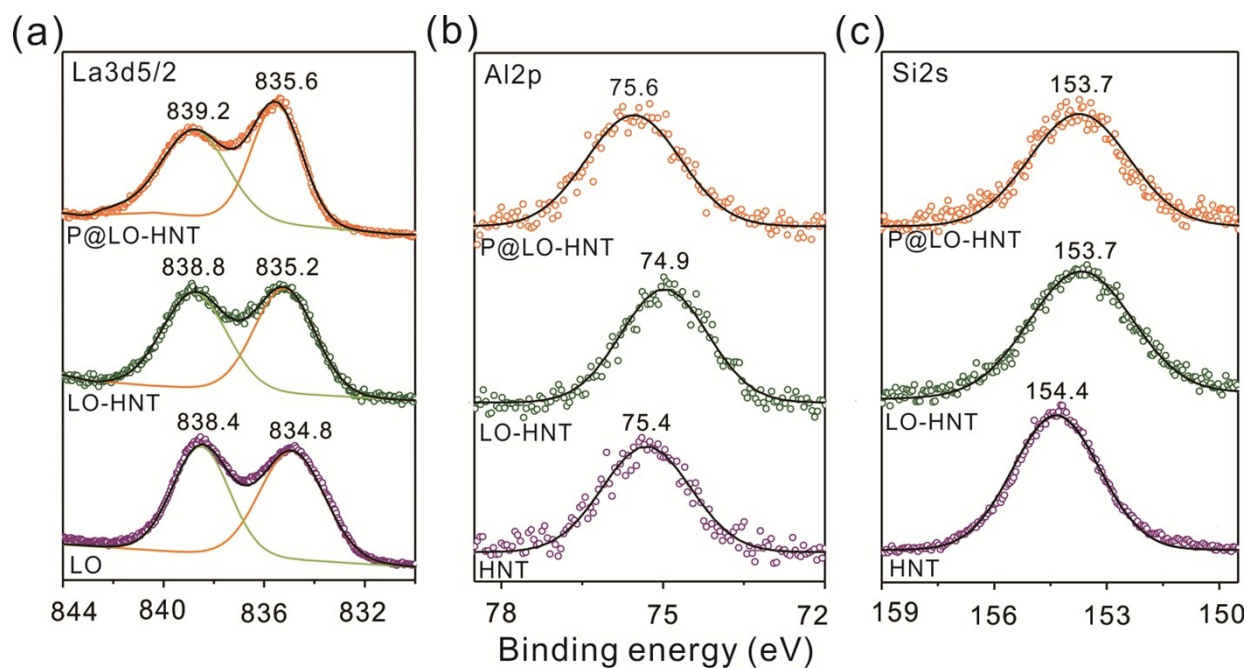


Figure S1 (a) XPS spectra of La_{3d5/2} for P@LO-HNT, LO-HNT and LO. (b) High-resolution XPS spectra of Al_{2p} in HNT, LO-HNT and P@LO-HNT, (c) High-resolution XPS spectra of Si_{2s} in HNT, LO-HNT and P@LO-HNT. The circles and solid lines denote the measured and smoothed XPS spectra respectively, and the values denote binding energies of La, Al and Si. All the intensities are normalized to the maximum intense peak within the respective spectral region.

XPS analysis further confirms the LO grafting on the surface of the HNT. The high-resolution La 3d_{5/2} XPS spectrum (Figure S2a) of pure LO shows the representative peaks of La 3d_{5/2} are centered at 834.8 and 838.4 eV. In the spectrum of LO-HNT, the binding energies of the La 3d_{5/2} shifted to higher value energies (835.2 and 838.8 eV) reflecting the

interaction of the deposited LO with surface Al and Si in HNT. The Al 2P peak of HNT is positioned at 75.4 eV, and this was shifted to 74.9 eV in LO-HNT (Figure S2b). At the same time, the Si 2s peak of HNT, positioned at 154.4eV, was shifted to 153.7 eV in LO-HNT (Figure S2c). These distinct binding energy shifts reflect the formation of Si–O–La and Al–O–La bonds for the La-HNT.

XPS characterizations of P@LO-HNT further identified the frequency of surface complexation, i.e., the phosphate adsorption mechanism. The peak of La 3d_{5/2} for P@LO-HNT is shifted to higher binding energies (at approximately 835.6 and 839.2eV; Figure S2a) versus the as-synthesized LO-HNT. This shift indicates electron transfer in the valence band of La 3d_{5/2} forms a La-O-P bond—this occurs at the surface of the coated LO nanoparticles. In addition, the Al 2p peak (at 74.9 eV) in the spectrum of LO-HNT (Figure S2b) shifts to 75.6 eV in P@LO-HNT suggesting that interactions occurred between Al and P by forming an Al-O-P bond, which likely occurred near the inner surface of HNT. These energy shifts are consistent with the values corresponding to the related interactions in the literature^{3,4} and provide evidence for the adsorption of phosphate by surface complexation. However, the Si 2s spectra of P@LO-HNT does not show obvious changes versus LO-HNT (Figure S2c). This suggests that the silicon in LO-HNT is inactive for phosphate adsorption.

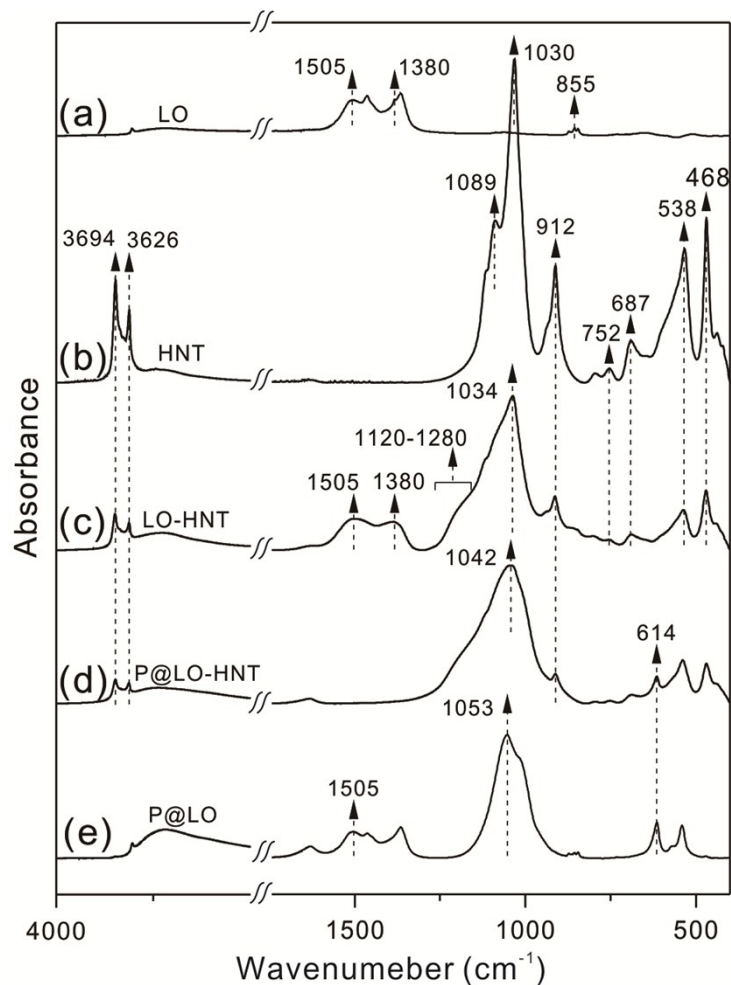


Figure S2 The FTIR spectra for (a) LO, (b) HNT, (c) LO-HNT, (d) phosphate adsorbed LO-HNT (P@LO-HNT), and (e) phosphate adsorbed LO (P@LO). The P@LO and P@LO-HNT were prepared at phosphate concentrations of 700 and 1000 mg P/L, respectively; the pH was 4.5. The preparation method were further used for XPS, FIB/TEM and P XANES

characterization.

The structural changes of HNT after LO coating were examined using FTIR. The vibrational bands (e.g. 1505, 1380 and 855 cm^{-1}) in the FTIR spectrum (Figure S1a) of LO are assigned to vibrations of CO_3^{2-} .⁵ Versus pristine HNT (Figure S1b), the LO-HNT has an increase in the intensity of the band at 1120 to 1280 cm^{-1} and new vibrational bands at 1505 and 1380 cm^{-1} (Figure S1c) indicating the presence of an Si–O–La bond⁶ and CO_3^{2-} vibrations in LO-HNT. The vibration bands at 3694, 3626, and 912 cm^{-1} were assigned to the

Al–OH vibrations of HNT⁷ and were much less distinct in LO-HNT than in HNT. This indicates dehydroxylation and related structural changes in halloysite. Moreover, the hybrid shows a significant weakening of the peaks of Si–O vibrations (at 1089, 1030, 752, 687, and 468 cm⁻¹) and Al–O–Si vibrations (538 cm⁻¹), suggesting a disconnect between tetrahedral SiO₄ and octahedral AlO₆ in the HNT unit. Thus, there is phase separation of SiO₂ and Al₂O₃—both of which are amorphous nanoparticles.⁸

The FTIR spectra indicate significant changes in the functional group chemistry of P@LO-HNT. Figure S1d shows the O–P–O bending vibration at 614 cm⁻¹ and the P–O stretching at 1053 cm⁻¹. These overlap with the Si–O–Si vibration at 1034 cm⁻¹ in HNT accompanied by the disappearance of vibrations of CO₃²⁻. This indicates the complete replacement of the exchangeable CO₃²⁻ groups between (La₂O₂²⁺)_n layers of LO by H₂PO₄⁻, which is the dominant phosphate species at pH 4.5⁹, i.e., an ion exchange occurs at interlayers of LO after phosphate adsorption. In contrast to the complete CO₃²⁻–H₂PO₄⁻ exchange for LO-HNT, the intensities of the vibrations of CO₃²⁻ in the spectrum of P@LO decreased only slightly (Figure S1e). This indicates the CO₃²⁻–H₂PO₄⁻ exchange ratio is low, because the pure phase of LO nanoparticles are aggregated (TEM in Figure S6). Thus, there is inefficient H₂PO₄⁻ exchange; however, the LO nanoparticles are well dispersed and the inner and outer surfaces of the HNT facilitates exchange.

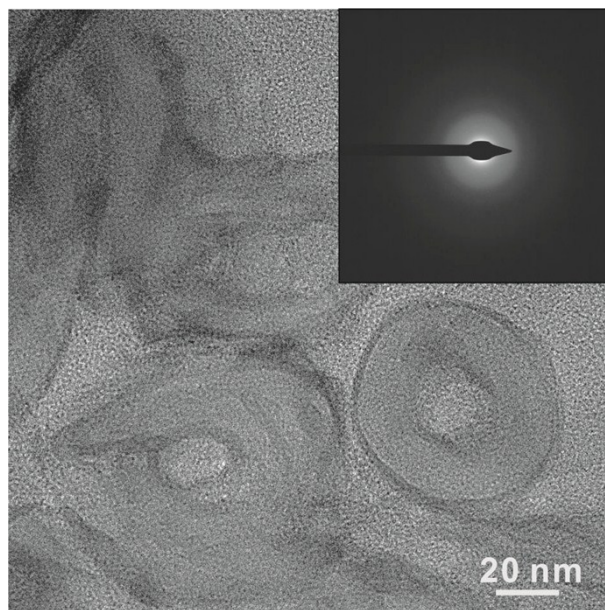


Figure S3 Cross-sectional TEM image of LO-HNT; inset: selected area electron diffraction (SAED) pattern, revealing the amorphous nature of the co-calcined HNT at 450°C.

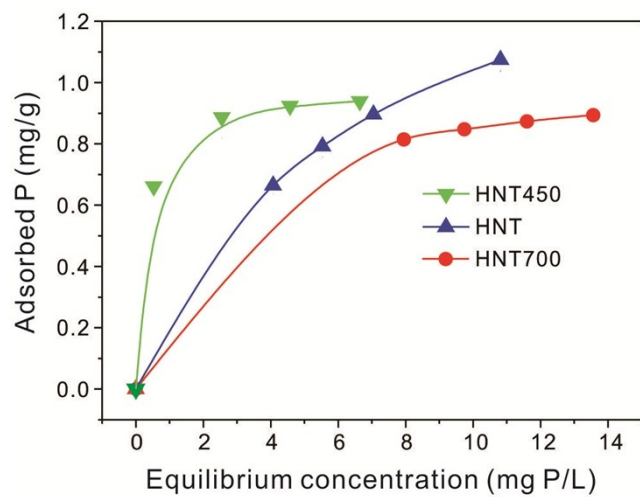


Figure S4 Phosphate adsorption isotherms for HNT and calcined HNT (at 450 and 700°C).

The solid lines are the fitted Langmuir adsorption isotherms.

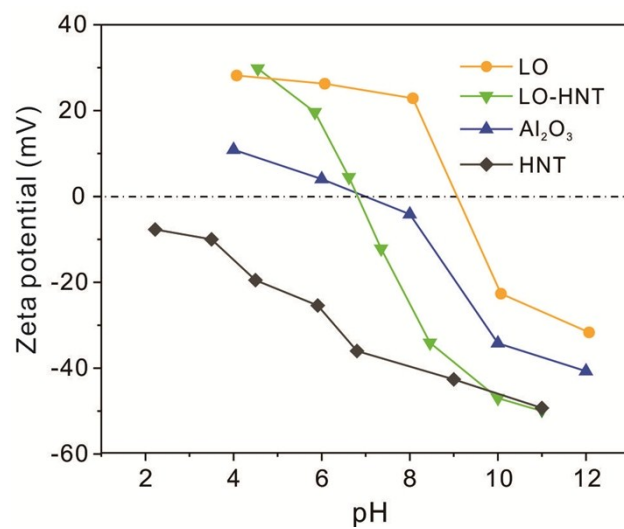


Figure S5 Zeta potential of LO-HNT, Al₂O₃, HNT, and LO as a function of pH.

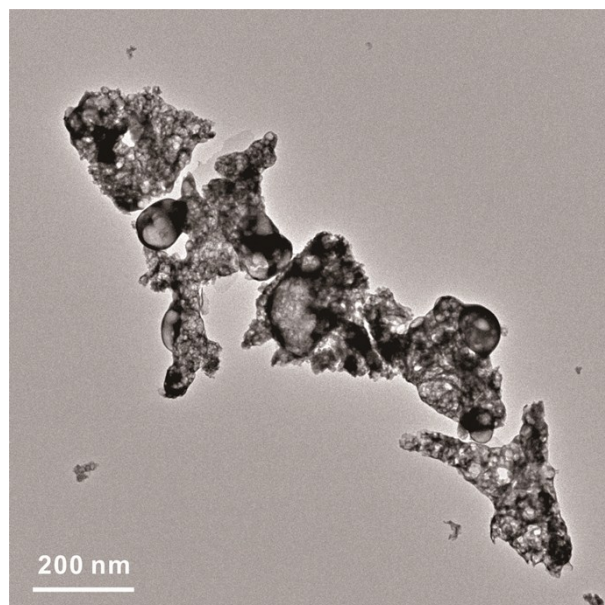


Figure S6. TEM images of LO nanoparticles.

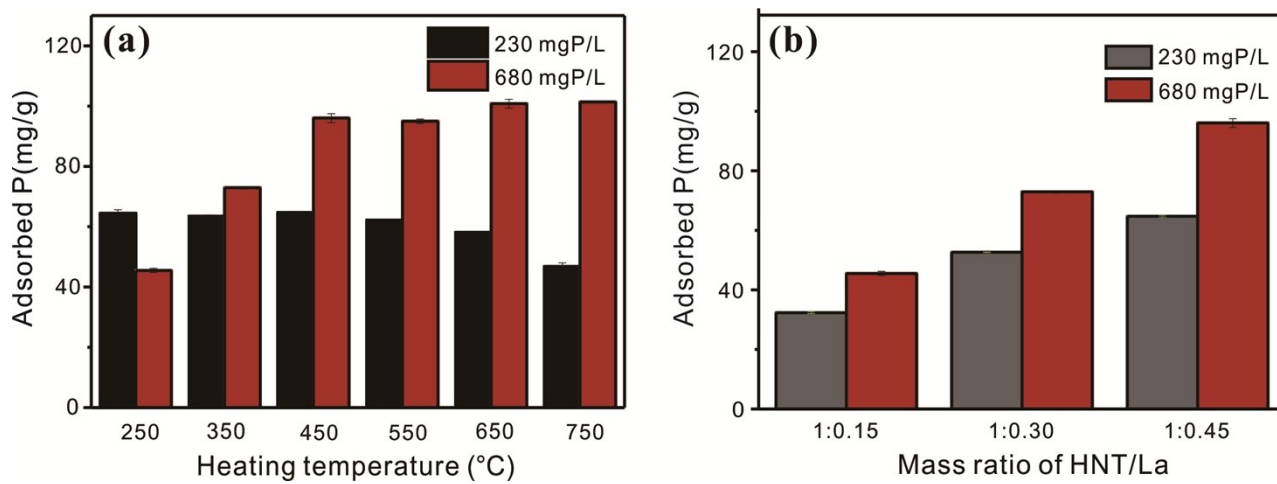


Figure S7. Effect of (a) different heating temperature and (b) mass ratio of HNT/La on phosphate removal.

Analysis for phosphate proportions of different states in LO-HNT

LCF analysis (Figure 5) shows that the amount of P adsorbed by LO nanoparticles and Al_2O_3 nanoparticles accounts for 76% and 24% of the total P content in the P@LO-HNT sample, respectively. The XRF result shows that the total amount of P in the P@LO-HNT sample is 7.29 mol%. Hence, we concluded from the LCF and XRF data that the content of P adsorbed to LO and Al_2O_3 are 5.54 mol% and 1.75 mol%, respectively. The XRF data of P @ LO-HNT shows that the amount of La is 4.56 mol%; and the amount of CO_3^{2-} is 2.28 mol%. Meanwhile, CO_3^{2-} is fully exchanged by a double portion of H_2PO_4^- ion. Thus, the 2.28 mol% of CO_3^{2-} can fully exchange 4.56 mol% of H_2PO_4^- . The XPS and FTIR analysis of P@LO-HNT samples shows two parts to the LO nanoparticle phosphate adsorption process: 1) exchange of CO_3^{2-} - H_2PO_4^- in the interlayer of LO and surface complexation of phosphate via La on the LO surface. Therefore, the amount of P on the surface complexation in LO is 0.98 mol% as calculated by subtracting the amount of CO_3^{2-} that was exchanged from P (4.56 mol%) In summary, the amount of P adsorbed by CO_3^{2-} - H_2PO_4^- exchange, phosphate complexation with La and Al site in LO-HNT are 4.56 mol%, 1.75 mol%, and 0.98 mol% respectively. The proportion of P adsorbed by CO_3^{2-} - H_2PO_4^- exchange and phosphate complexation with La and Al are 62.6%, 13.4% and 24%, respectively.

Table S1. XRF result of LO-HNT and P@LO-HNT sample shown in mass ratio and molar fraction.

Composition	LO-HNT			P@LO-HNT				
	Mass (%)	fraction	Mole (%)	fraction	Mass (%)	fraction	Mole (%)	fraction
Al	15.17		15.14		11.84		11.26	
Si	15.83		15.17		11.56		10.56	
O	35.78		60.21		40.02		64.25	
La	31.39		6.08		24.67		4.56	
C	1.35		3.03		-		-	
Fe	0.10		0.05		0.02		0.01	
Ca	0.12		0.08		0.08		0.05	
Mg	0.07		0.08		0.04		0.04	
K	0.09		0.05		2.89		1.89	
Na	0.09		0.11		0.08		0.09	
P	-		-		8.80		7.29	

Table S2. The maximum phosphate adsorption capacity (Q_m) of La-coated materials reported in the literature.

Materials	Q_m (mg P/g)	Refs.
La(III)-chelex resin	2.9	10
La-silica	3.44	11
La-ACF	5.85	12
La-Phoslock	10.6	13
La-lignocellulose	10.8	14
La-orange waste	13.9	15
La(III)-bentonite	14	16
La-mesoporous silicates	22	17
La-mesoporous SiO ₂	23.1	18
La/Fe-activated carbon fiber	29.4	19
La-porous carbon	32.4	20
La-CuFe ₂ O ₄	32.6	21
M-La(OH) ₃	52.7	22
La-biochar	46.4	23
Mag@Fh-La	44.8	22
La-linked polystyrene	57.4	24
La/Al-Hydroxide Composite	71.6	25
La-zeolite	71.9	26
Fe-La-porous silica	72.0	27
La-silica foams	70.4	28
La(OH) ₃ -activated carbon fiber	16.1	29
Lanthanum-mesoporous silica	42.8	30

La-SBA	45.6	31
La ₂ O ₃ @Fe ₃ O ₄ @SiO ₂	27.8	32
La- vermiculites	79.6	33
La-zeolite	24.6	34
La-Al montmorillonite	13.02	35
La-hybrid film	42.7	36
La-graphene	82.6	37
La-ceramic	0.89	38
La-NN-M41	54.3	39
La-vesuvianite	20.5	40
La-bentonite	9.2	41
La-silica spheres	47.9	42
La-carbon nanotube	48.0	43
La-mesoporous ilicates	54.3	39
La-zeolites	58.2	44
La-graphene	82.6	37
La(OH) ₃ /Fe ₃ O ₄	83.5	45
La-cationic hydrogel	90.2	9
La-zeolite	99.0	46
La- tourmaline	108.7	47
LO-HNT	130.4	The present study

Table S3. Langmuir parameters fitted for adsorption isotherm of LO, HNT, LO-HNT, and HNT calcined at 450°C and 700°C, respectively.

Sample	K_L	Q_m	R^2
HNT	0.155	1.71 (mg P/g)	99.99
LO	0.003	173.2 (mg P/g La)	98.85
LO-HNT	0.006	415.4 (mg P/g La)	99.86
LO-HNT	0.006	130.4 (mg P/g)	99.86
HNT 450°C	3.952	1.14 (mg P/g)	97.50
HNT 700°C	0.459	1.04 (mg P/g)	99.99

Table S4 Parameter of the sewage effluent sampled from a subsurface flow constructed wetlands within the campus of Guangzhou Institute of Geochemistry, Guangzhou City, China.

pH	DO ^a	TOC ^b	COD ^c	TP ^d	NO ₃ -N ^e	NH ₄ -N ^f	TN ^g
7.96	0.15	41.80	174.40	2.30	0.20	29.70	55

^aDissolved oxygen, mg/L; ^bTotal organic carbon, mg/L; ^cchemical oxygen demand, mg/L; ^dtotal phosphorus, mg/L; ^eNitrate nitrogen; ^fammonium, mg/L. ^gTotal nitrogen.

Table S5 Dose of reported phosphate adsorbents used in actual sewage for phosphate adsorption in literature.

Adsorbents	Initial phosphorus concentration (mg/L)	Removal efficiency (%)	Adsorbent dose (mg/L)	References
La-vesuvianite	0.94	100	0.30	40
Zr-MOF	1.77	100	0.10	48
La(OH) ₃ -PLNFs	2	100	1	49
Fe ₃ O ₄ @SiO ₂	1.9	95	0.20	32
MnO ₂	1.48	100	0.25	50
La-silica	2	99.71	0.042	42
MgCl ₂ -alginate biochar	1.82	>54.6%	2	51
La-MOF	0.50	95.81	0.08	52
La-Fe(OH) ₃	5	70–90%	0.5	45
Mag@Fh-La	1.70	98.80	0.20	22
Fe ₃ O ₄ @ZnO	2.10	97.60	0.30	53
LO-HNT ^a	2.30	100	0.05	The present study

Supporting References

- [1] L. M. Cornaglia, J. Múnera, S. Irusta, E. A. Lombardo, *Applied Catalysis A: General* **2004**, *263*, 91–101.
- [2] N. Liu, Z. Wu, M. Li, S. Li, Z. Luo, Y. Li, L. Pan, Y. Liu, *ChemCatChem* **2017**, *9*, 1641–1647.
- [3] P. Yuan, P. D. Southon, Z. Liu, M. E. R. Green, J. M. Hook, S. J. Antill, C. J. Kepert, *The Journal of Physical Chemistry C* **2008**, *112*, 15742–15751.
- [4] P. Yuan, D. Tan, F. Aannabi-Bergaya, W. Yan, M. Fan, D. Liu, H. He, *Clays and Clay Minerals* **2012**, *60*, 561–573.
- [5] S. Dong, Y. Wang, Y. Zhao, X. Zhou, H. Zheng, *Water Research* **2017**, *126*, 433–441.
- [6] E. W. Shin, J. S. Han, M. Jang, S.-H. Min, J. K. Park, R. M. Rowell, *Environ. Sci. Technol.* **2004**, *38*, 912–917.
- [7] L. Fang, Q. Shi, J. Nguyen, B. Wu, Z. Wang, I. M. C. Lo, *Environ. Sci. Technol.* **2017**, *51*, 12377–12384.
- [8] R. S. S. Wu, K. H. Lam, J. M. N. Lee, T. C. Lau, *Chemosphere* **2007**, *69*, 289–294.
- [9] E. W. Shin, K. G. Karthikeyan, M. A. Tshabalala, *Environ. Sci. Technol.* **2005**, *39*, 6273–6279.
- [10] B. K. Biswas, K. Inoue, K. N. Ghimire, S. Ohta, H. Harada, K. Ohta, H. Kawakita, *Journal of Colloid and Interface Science* **2007**, *312*, 214–223.
- [11] V. Kuroki, G. E. Bosco, P. S. Fadini, A. A. Mozeto, A. R. Cestari, W. A. Carvalho, *Journal of Hazardous Materials* **2014**, *274*, 124–131.
- [12] J. Zhang, Z. Shen, W. Shan, Z. Chen, Z. Mei, Y. Lei, W. Wang, *Journal of Environmental Sciences* **2010**, *22*, 507–511.
- [13] E. Ou, J. Zhou, S. Mao, J. Wang, F. Xia, L. Min, *Colloids and Surfaces A: Physicochemical and Engineering Aspects* **2007**, *308*, 47–53.
- [14] J. Liu, Q. Zhou, J. Chen, L. Zhang, N. Chang, *Chemical Engineering Journal* **2013**, *215–216*, 859–867.
- [15] P. Koilraj, K. Sasaki, *Chemical Engineering Journal* **2017**, *317*, 1059–1068.
- [16] W. Gu, X. Li, M. Xing, W. Fang, D. Wu, *Science of The Total Environment* **2018**, *619–620*, 42–48.
- [17] Z. H. Wang, D. K. Shen, F. Shen, T. Y. Li, *Chemosphere* **2016**, *150*, 1–7.
- [18] Y. Zhang, B. Pan, C. Shan, X. Gao, *Environmental Science & Technology* **2016**, *50*, 1447–1454.
- [19] R. Xu, M. Zhang, R. J. G. Mortimer, G. Pan, *Environ. Sci. Technol.* **2017**, *51*, 3418–3425.
- [20] J. Xie, Z. Wang, D. Fang, C. Li, D. Wu, *Journal of Colloid and Interface Science* **2014**, *423*, 13–19.
- [21] C. Wang, X. Zheng, F. Zhang, Y. Huang, J. Pan, *RSC Advances* **2016**, *6*, 87808–87819.
- [22] J. Yang, P. Yuan, H.-Y. Chen, J. Zou, Z. Yuan, C. Yu, *Journal of Materials Chemistry* **2012**, *22*, 9983–9990.
- [23] L. Zhang, Q. Zhou, J. Liu, N. Chang, L. Wan, J. Chen, *Chemical Engineering Journal* **2012**, *185–186*, 160–167.
- [24] W. Y. Huang, X. Yu, J. P. Tang, Y. Zhu, Y. M. Zhang, D. Li, *Microporous And Mesoporous Materials* **2015**, *217*, 225–232.
- [25] J. Yang, L. Zhou, L. Zhao, H. Zhang, J. Yin, G. Wei, K. Qian, Y. Wang, C. Yu, *J. Mater. Chem.* **2011**, *21*, 2489–2494.
- [26] W. Huang, Y. Zhu, J. Tang, X. Yu, X. Wang, D. Li, Y. Zhang, *Journal of Materials Chemistry A* **2014**, *2*, 8839–8848.
- [27] E. Zong, X. Liu, J. Wang, S. Yang, J. Jiang, S. Fu, *J Mater Sci* **2017**, *52*, 7294–7310.

- [28] J. Zhang, Z. Shen, W. Shan, Z. Mei, W. Wang, *Journal of Hazardous Materials* **2011**, *186*, 76–83.
- [29] J. Goscianska, M. Ptazkowska-Koniarz, M. Frankowski, M. Franus, R. Panek, W. Franus, *Journal of Colloid and Interface Science* **2018**, *513*, 72–81.
- [30] M. Chen, C. Huo, Y. Li, J. Wang, *ACS Sustainable Chemistry & Engineering* **2016**, *4*, 1296–1302.
- [31] B. Wu, L. Fang, J. D. Fortner, X. Guan, I. M. C. Lo, *Water Research* **2017**, *126*, 179–188.
- [32] Z. Wang, Y. Fan, Y. W. Li, F. R. Qu, D. Y. Wu, H. N. Kong, *Microporous And Mesoporous Materials* **2016**, *222*, 226–234.
- [33] H. Liang, K. Liu, Y. Ni, *Journal of the Taiwan Institute of Chemical Engineers* **2017**, *71*, 474–479.
- [34] R. Mallampati, S. Valiyaveetil, *Acs Applied Materials & Interfaces* **2013**, *5*, 4443–4449.
- [35] L. Chen, X. Zhao, B. Pan, W. Zhang, M. Hua, L. Lv, W. Zhang, *Journal of Hazardous Materials* **2015**, *284*, 35–42.
- [36] D. Mitrogiannis, M. Psychoyou, I. Baziotis, V. J. Inglezakis, N. Koukouzas, N. Tsoukalas, D. Palles, E. Kamitsos, G. Oikonomou, G. Markou, *Chemical Engineering Journal* **2017**, *320*, 510–522.
- [37] J. Chen, L. G. Yan, H. Q. Yu, S. Li, L. L. Qin, G. Q. Liu, Y. F. Li, B. Du, *Chemical Engineering Journal* **2016**, *287*, 162–172.
- [38] F. Xie, F. Wu, G. Liu, Y. Mu, C. Feng, H. Wang, J. P. Giesy, *Environmental Science & Technology* **2014**, *48*, 582–590.
- [39] L. Fang, B. Wu, I. M. C. Lo, *Chemical Engineering Journal* **2017**, *319*, 258–267.
- [40] H. Qiu, C. Liang, X. Zhang, M. Chen, Y. Zhao, T. Tao, Z. Xu, G. Liu, *Acs Applied Materials & Interfaces* **2015**, *7*, 20835–20844.
- [41] M. Rashid, N. T. Price, M. Á. Gracia Pinilla, K. E. O’Shea, *Water Research* **2017**, *123*, 353–360.
- [42] W. H. Xiong, J. Peng, *Water Research* **2008**, *42*, 4869–4877.
- [43] W. Chouyyok, R. J. Wiacek, K. Pattamakomsan, T. Sangvanich, R. M. Grudzien, G. E. Fryxell, W. Yantasee, *Environmental Science & Technology* **2010**, *44*, 3073–3078.
- [44] X. Wang, L. Dou, Z. Li, L. Yang, J. Yu, B. Ding, *ACS Appl. Mater. Interfaces* **2016**, *8*, 34668–34676.
- [45] L. Fang, R. Liu, J. Li, C. Xu, L.-Z. Huang, D. Wang, *Water Research* **2018**, *130*, 243–254.
- [46] R. Chitrakar, S. Tezuka, J. Hosokawa, Y. Makita, A. Sonoda, K. Ooi, T. Hirotsu, *Journal of Colloid and Interface Science* **2010**, *349*, 314–320.
- [47] J. Zhou, Z. P. Xu, S. Qiao, Q. Liu, Y. Xu, G. Qian, *Journal of Hazardous Materials* **2011**, *189*, 586–594.
- [48] K. Kuzawa, Y.-J. Jung, Y. Kiso, T. Yamada, M. Nagai, T.-G. Lee, *Chemosphere* **2006**, *62*, 45–52.
- [49] X. Ge, X. Y. Song, Y. Ma, H. J. Zhou, G. Z. Wang, H. M. Zhang, Y. X. Zhang, H. J. Zhao, P. K. Wong, *Journal of Materials Chemistry A* **2016**, *4*, 14814–14826.
- [50] N. Pitakteeratham, A. Hafuka, H. Satoh, Y. Watanabe, *Water Research* **2013**, *47*, 3583–3590.
- [51] E. Zong, D. Wei, H. Wan, S. Zheng, Z. Xu, D. Zhu, *Chemical Engineering Journal* **2013**, *221*, 193–203.
- [52] H. Li, J. Ru, W. Yin, X. Liu, J. Wang, W. Zhang, *Journal of Hazardous Materials* **2009**, *168*, 326–330.
- [54] Y. Gu, D. Xie, Y. Ma, W. Qin, H. Zhang, G. Wang, Y. Zhang, H. Zhao, *ACS Appl. Mater. Interfaces* **2017**, DOI 10.1021/acsami.7b10024.

- [55] J. He, W. Wang, F. Sun, W. Shi, D. Qi, K. Wang, R. Shi, F. Cui, C. Wang, X. Chen, *ACS Nano* **2015**, *9*, 9292–9302.
- [56] L. Lai, Q. Xie, L. N. Chi, W. Gu, D. Y. Wu, *Journal of Colloid and Interface Science* **2016**, *465*, 76–82.